64670

REPORT DOCUMENTATION PAGE

AFRL-SR-AR-TR-02-

0207

1. AGENCY USE ONLY (Leave blank)	2. REPORT DATE	3. REPORT TYPE AND DATES COVERED
	6/5/2002	Final 7/1/1996 - 9/30/1999

4. TITLE AND SUBTITLE

AASERT '96 - Applications of Porous Glass Based Thick Holograms for Optical Data Storage and Narrow-Band Wave Length Filtering

5. FUNDING NUMBERS

F49620-96-1-0308
3484/YS
61103D

6. AUTHOR(S)

Prof. Shaoul Ezekiel, Dr. Selim Shahriar

7. PERFORMING ORGANIZATION NAME(S) AND ADDRESS(ES)

Research Laboratory of Electronics
Massachusetts Institute of Technology
77 Massachusetts Avenue
Cambridge, MA 02139

8. PERFORMING ORGANIZATION REPORT NUMBER

9. SPONSORING/MONITORING AGENCY NAME(S) AND ADDRESS(ES)

AFOSR/PKA
110 Duncan Avenue, Room B115
Bolling AFB, DC 20332-8080

10. SPONSORING/MONITORING AGENCY REPORT NUMBER

3484/YS

11. SUPPLEMENTARY NOTES

The view, opinions and/or findings contained in this report are those of the author(s) and should not be construed as an official Department of the Army position, policy, or decision, unless so designated by other documentation.

12a. DISTRIBUTION/AVAILABILITY STATEMENT

Approved for public release; distribution unlimited.

12b. DISTRIBUTION CODE

13. ABSTRACT *(Maximum 200 words)*

Under this grant, our objective was to test the feasibility of realizing holographic optical memory.

20020719 131

14. SUBJECT TERMS			15. NUMBER OF PAGES
			16. PRICE CODE
17. SECURITY CLASSIFICATION OF REPORT	18. SECURITY CLASSIFICATION OF THIS PAGE	19. SECURITY CLASSIFICATION OF ABSTRACT	20. LIMITATION OF ABSTRACT
UNCLASSIFIED	UNCLASSIFIED	UNCLASSIFIED	UL

Applications of Porous Glass Based Thick Holograms for Optical Data Storage and Narrow-Band Wave Length Filtering

FINAL REPORT

OSP#: 6467000
Contract #: F49620-96-1-0308

Co-Principal Investigators:
Prof. Shaoul Ezekiel and Dr. Selim Shahriar
Research Laboratory of Electronics
Massachusetts Institute of Technology
Cambridge, MA 02139

A. Objectives:

Under this grant, our objective was to test the feasibility of realizing holographic optical memory.

B. Accomplishments/New Findings:

B.1. Observation of Raman Induced Spin Echoes

Basic Model for Raman Excited Spin Echoes in a Three-level System

Consider a Λ-type three-level optical medium interacting with two Raman resonant frequencies, ω_1 and ω_2 (Figure 1(a)). Ideally, the two ground states are long lived and the excited state is short lived. In this case, after a few optical pumping cycles, a Raman "dark state" is formed. However, because the Raman resonant fields are not co-propagating, the relative phases of the two ground state contributions to this dark state depend on position. This creates a grating-like structure. Readout of this grating can be accomplished using a single, near resonant probe beam at ω_3 that is Bragg matched to diffract into an output beam at ω_4 via nondegenerate four wave mixing (NDFWM). By tuning the probe beam slightly off-resonance, or to another excited state, higher diffraction efficiency can be achieved.

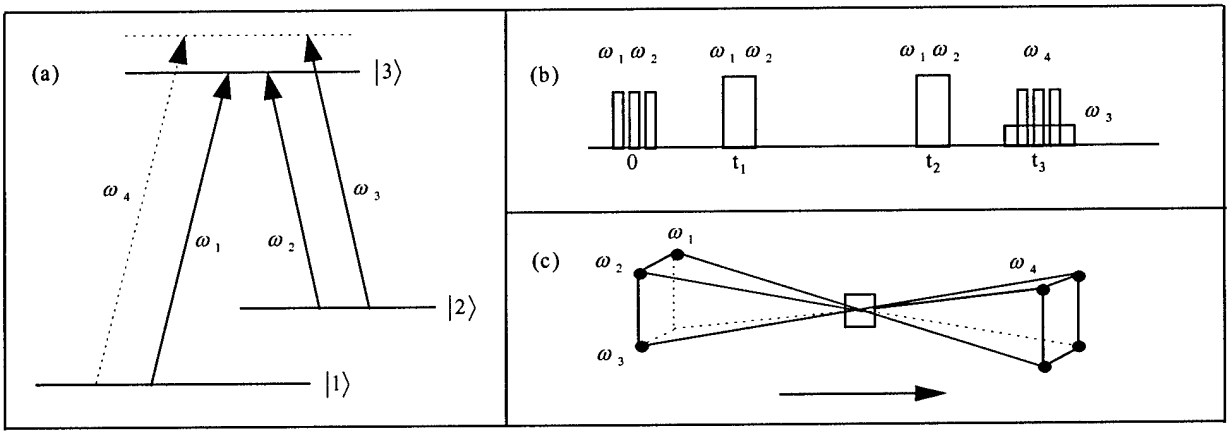

Figure 1. (a) Enhanced NDFWM detection of Raman excited spin coherence. (b) Pulse sequence for Raman excited spin echoes. (c) Background-free detection of Raman excited spin echoes using NDFWM.

When the long-lived ground states are magnetic sublevels, the Raman dark state is equivalent to a spin coherence excited by an rf field of appropriate phase. The dark state

grating is therefore a spin orientation grating that is capable of diffracting light. In a material with an inhomogeneously broadened spin transition, this spin grating can dephase. However, it is possible to re-phase the grating by applying an rf or Raman pulse, just as in spin echoes. Therefore, using Raman resonant light, spin echoes can be optically excited and optically probed by NDFWM. Moreover, high resolution optical holography can be performed with spin echoes.

A representative pulse sequence for the Raman excited spin echo storage of a stream of binary optical data bits is shown in Figure 1(b). Here, optical data is input as a series of non-copropagating object and reference beam pulses, containing both ω_1 and ω_2. The intense write beam is also composed of (plane wave) ω_1 and ω_2 beams. The case shown corresponds to a stimulated spin echo, so that a read pulse is required. The read pulse is also composed of plane wave ω_1 and ω_2 beams. Finally, to probe the resulting spin echo, a Bragg matched probe beam at ω_3 is applied at the appropriate time to generate the readout beam at ω_4 via NDFWM.

Raman Dark State in a Rare-earth Doped Solid, Pr^{3+}:Y_2SiO_5

Very recently, Raman dark states were observed in ruby with a high power pulsed laser and in a rare-earth doped crystal, Pr^{3+}:Y_2SiO_5 (Pr:YSO) with low power of a cw laser. Figure 2 shows Raman dark states in Pr:YSO. The optical transition is $^3H_4 \rightarrow {}^1D_2$ (λ = ~ 605 nm). This data was obtained using a frequency stabilized cw ring dye laser of ~ 1MHz linewidth with maximum power (in the ω_2 beam) of 54 mW. The data traces in Figure 2(a)-(d) corresponded to laser powers of 1.6, 5, 16, and 50 mW respectively. For this data, the probe field ω_1 is scanned through the two-photon (Raman) resonance frequency while its absorption is monitored. The separation between states $|1\rangle$ and $|2\rangle$ in Fig. 1 is 10.2 MHz. The actual system in Pr:YSO is composed of 3 magnetic spin sublevels on each of the ground and excited states. To prevent all the population from being trapped in the third ground state sublevel, we used a "repump" beam that excites a transition from the third ground state (not shown) to an excited state different from the one excited by ω_1 and ω_2. The width of the observed transparency in Figure 2 is as narrow as 15 kHz, which is much less than the 1 MHz laser jitter. This sub-laser-jitter linewidth is the signature of the Raman excited dark state.

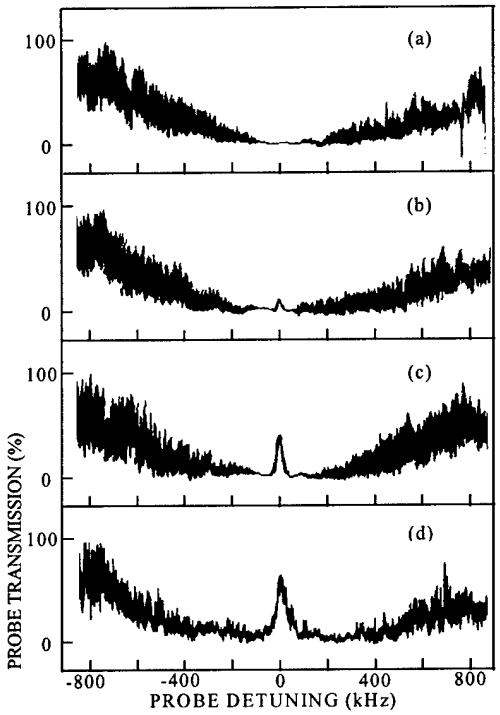

Figure 2. Raman dark state excitation in Pr^{3+}:Y_2SiO_5 at 2K.

Raman Excited Spin Echo in Pr^{3+}:Y_2SiO_5

Figure 3 shows the Raman excited spin echo in Pr:YSO at 5K. The pulse sequence is shown at the top of the figure. First, a repump pulse is applied. This is followed by two Raman resonant optical pulses (labeled Λ) of 8 μsec length and 42 μsec separation. To generate the data trace, a Bragg matched probe pulse is applied at various delay times and the intensity of the NDFWM signal is plotted as a function of delay time. A boxcar integrator is used to average out laser jitter effects. The first two peaks in Figure 3 arise from the spin free induction decay (FID) signal and the third peak is the echo signal. The echo efficiency is ~ 55 % of the FID signal.

Using Raman excited spin echoes the spin homogeneous lifetime can be measured. Figure 4(a) shows this spin lifetime (T_2) as a function of temperature. As can be seen, the spin lifetime does not depend strongly on temperature up to 6K. Figure 4(b) shows the spin echo efficiency (as measured by NDFWM) vs. temperature. As seen, above 4 °K, the echo efficiency decreases rapidly. This is due to broadening of the optical homogenous width by phonon interactions. Above 6 K, spin echoes were still observed, but the echo intensity was too weak for a reliable spin T_2 measurement. The data in Figure 4 clearly shows the potential of Raman excited spin echoes to increase the operating temperature of SHB materials.

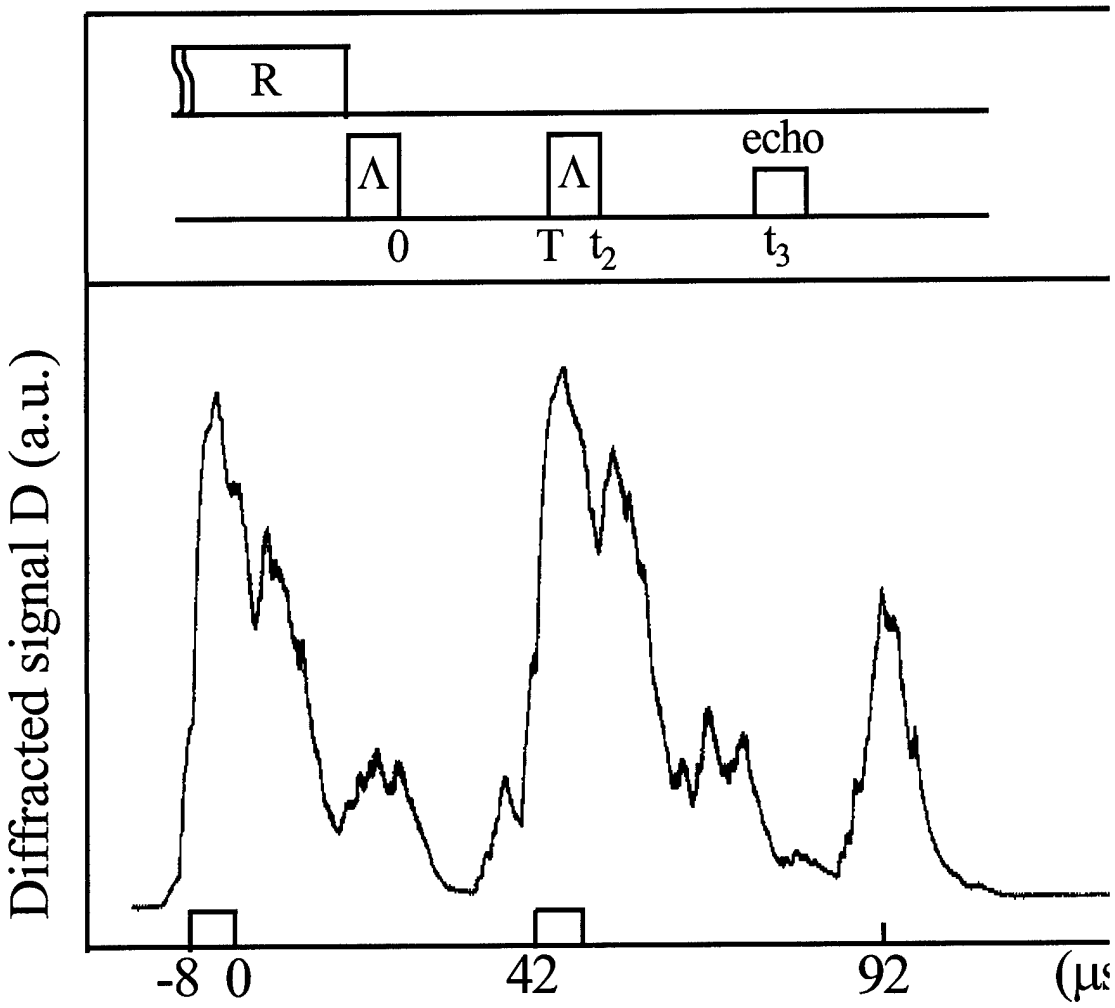

Figure 3. Raman excited spin echo in Pr:YSO.

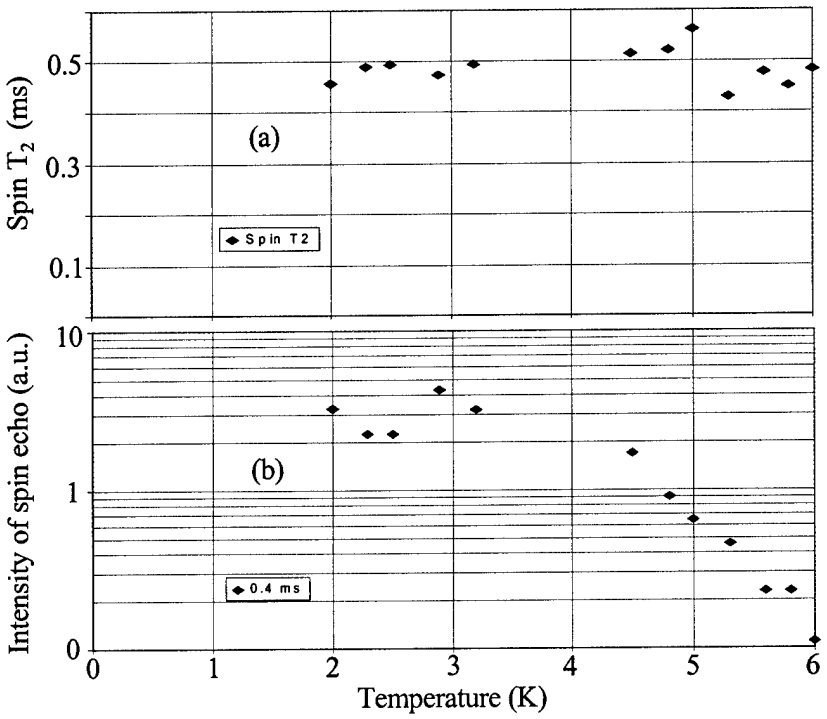

Figure 4 Temperature dependence of (a) spin T_2 and (b) intensity of echo signal

B.2 Demonstration of Frequency-selective Time-domain Data Storage using Raman Excited Spin Echoes

Figure 5 shows the storage of two bits of optical data using Raman excited spin echoes in Pr:YSO at 6 K. As mentioned already, each input pulse is composed of two Raman resonant frequencies, ω_1 and ω_2 (see Figure 3). The laser powers at ω_1 and ω_2 are ~ 30 mW and ~ 2 mW, respectively. To distinguish the data pulses d and d' (see Figure 5) from each other, the pulse widths are adjusted to be 7 μs and 2 μs, respectively. Because the pulse width contributes to pulse area, and both pulses are shorter than the spin inhomogeneous dephasing time, the resulting echoes are expected to have different amplitudes. This is observed in the echo signals of Figure 5. For this data, the write pulse delay time t_2 (400 μs) is chosen to be much longer than the optical T_2 (< 100 μs), so that no optical coherence survives. Similarly, the read pulse time delay t_3 (1500 μs) is chosen to be much longer than the spin T_2 (560 μs) so that no spin coherence survives. Thus, the second set of echoes in Figure 5 are stimulated echoes. The width of the optical frequency channel is determined by laser jitter and is ~ 1 MHz.

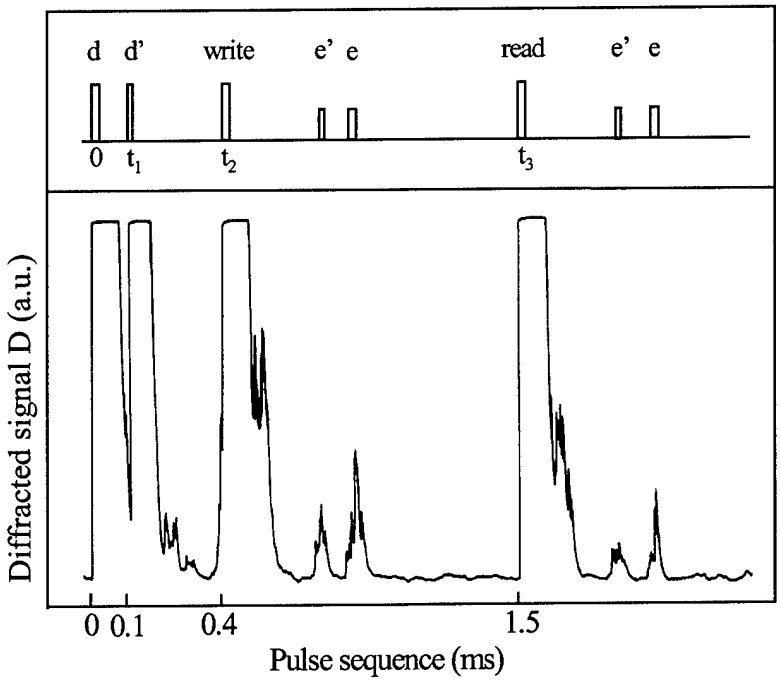

Figure 5 Optical data storage by EIT excited spin echo in Pr^{3+}:Y_2SiO_5.

Summary of Experimental Observations

We have already demonstrated experimentally that Raman excited spin coherences can be excited in a rare earth doped crystal of Pr:YSO with high efficiency. We have also demonstrated the generation of spin echoes with Raman resonant optical pulses and background-free detection with NDFWM. Using spin echoes, the spin homogeneous lifetime was measured and found to be independent of temperature up to 6K. In contrast, the optical homogeneous lifetime decreases rapidly above 4K. We also performed an optical data storage demonstration at 6K in which 2 bits of data were successfully stored and recalled using Raman excited stimulated spin echoes. Our studies have pointed out the following advantages of Raman excited spin echoes over conventional optical echoes:

- The spin T_2 is less sensitive to temperature.
- The Raman excited spin echo is less sensitive to the laser jitter.
- The Raman excited spin echo can be detected with high optical efficiency.

B.3. Frequency Domain Spectral Holeburning in Chlorin-e_6

We have studied frequency domain SHB in the organic dye called chlorin-e_6, doped in an amorphous host, in order to determine the feasibility of producing a one terabyte read-write long term memory system.

The first step in this process was the selection of the host material. In this selection process, we were guided by the following constraints:

- The dye must be soluble in the host to a level that yields an optical density of unity for a sample thickness of 0.5 to 1.0 cm
- The sample must be optically clear, with very low level of scattering
- The host must be either a glass (random structure) or a partially crystalline structure, in order to provide a widely varying molecular environment around each dye molecule
- The host should be relatively easy to handle and cast into samples of arbitrary shapes and sizes
- The host should be chemically inert with respect to the dye
- The host must have fundamental properties which allow for long storage life of the spectral hole
- The ratio of the inhomogeneous to homogeneous linewidths should be as high as possible (with a minimum value of 5000)

These requirements are generally well met by the common organic polymers polystyrene (PS), polymethylmethacrylate (PMMA), and polyvinyl alcohol (PVA). In fact, these three hosts have been used in a substantial fraction of all the SHB research studies, and have been used with most of the favored photochemical species. The reason for the favored use of these three hosts relates strongly to their ease of handling and preparation. Guided by detailed studies using these hosts , we chose PS as the first host to try.

Our basic approach for making samples of PS with Chlorin-e_6 (PSC) was simple. We melted pellets of PS in a beaker on a hot plate, added the dye (dissolved in dichloromethane), and stirred the mixture in order to produce an even distribution. The liquid PS was then poured onto an optical flat, enclosed by tapes, and then coverd by another flat. This approach had many pitfalls: the finished samples had bubbles in them, and the surfaces were concave. In order to eliminate these problems, we developed a special approach.

The bubbles were formed during the process of mixing the dye solution in the liquid PS. In order to drive the bubbles out, we placed the hot, molten PSC mixture in a special oven which could be pressurized with helium, as well as evacuated by a pump, alternatingly. This apparatus is shown in figure 7 . This approach yielded a uniform mixture of molten PSC at 160^{o} C,

THIS
PAGE
IS
MISSING
IN
ORIGINAL
DOCUMENT

Fig. 6

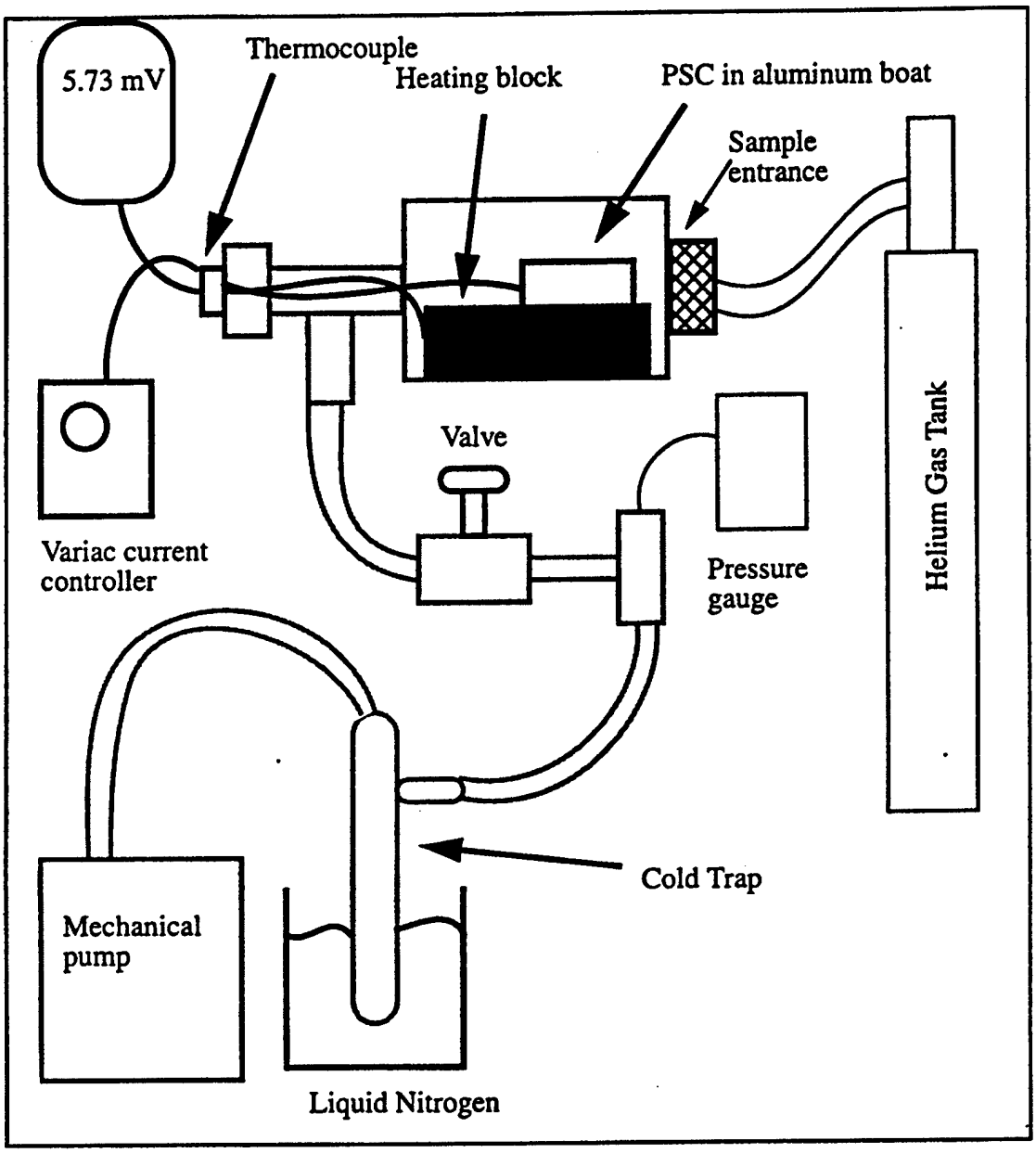

Figure 7. Pressure/Vacuum heating chamber for preaparation of bubble-free PSC mixture

free from any bubbles.

In order to eliminate the surface concavity, we designed a special press. This is illustrated schematically in figure 8. Briefly, a teflon O-ring was placed on an optical flat, and the hot, molten PSC was poured onto the flat, while under a glove-bag filled with helium, in order to prevent contamination and/or oxidation. A second flat was then placed on the O-ring, and pushed down with a press. The amount of pressure applied was varied manually during the cool-down period, by turning a screw. This process yielded samples that were free from any concavity.

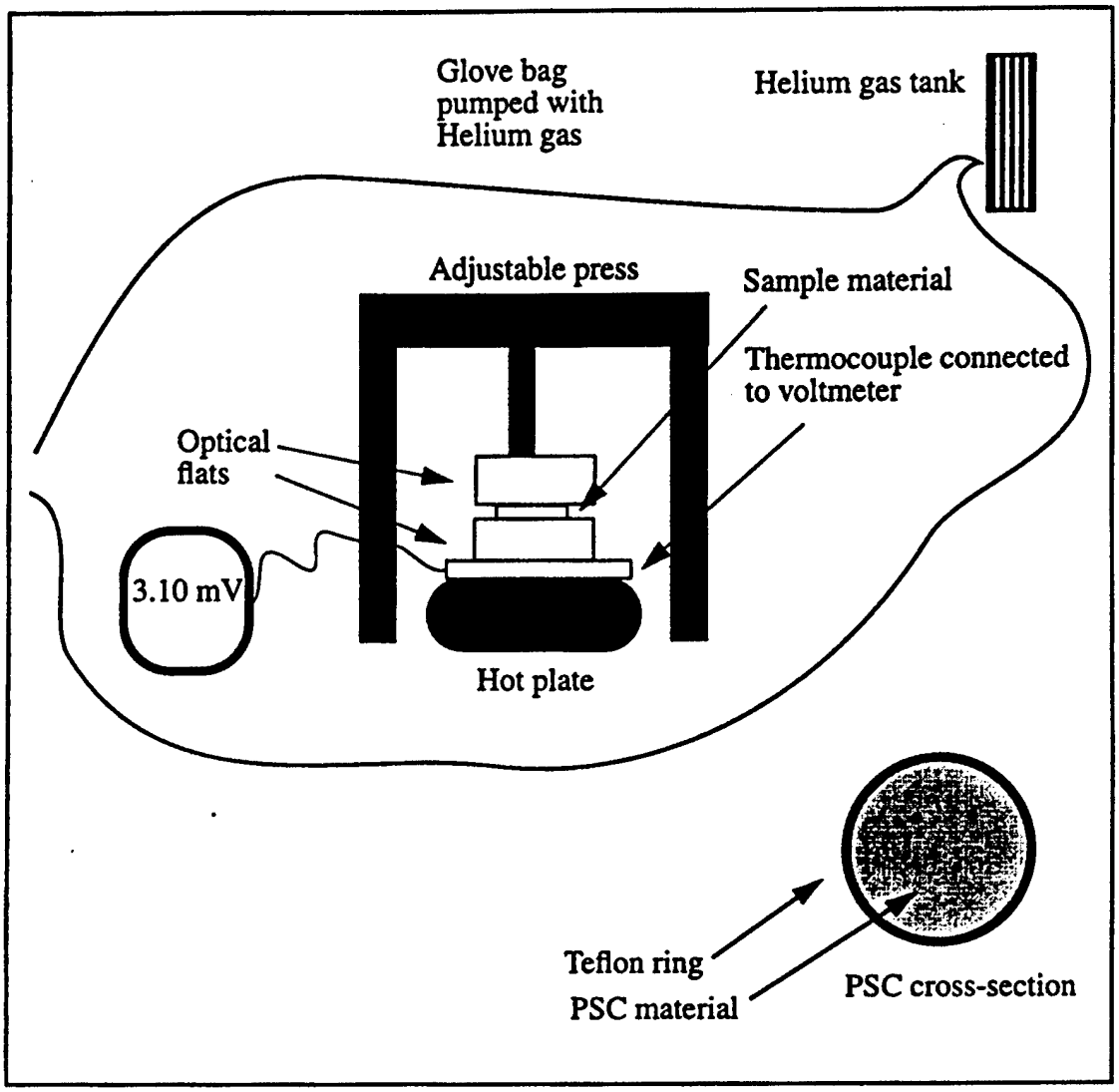

Figure 8. An adjustable press for producing concavity-free samples of PSC.

The optical quality samples produced this way were then placed in a cryostat, in order to study its spectral properties. The cryostat was designed in a manner such that the sample would not come in contact with the liquid helium; rather, it would be immersed in a helium gas, maintained at about 6 K. Figure 9 shows the basic mounting scheme, where the PSC sample, encased in a teflon O-ring, is held in place by two indium wire contact rings.

We used a 5 mwatts semiconductor laser, operated under external cavity feedback via a grating in the Littrow configuration (bought from Micracor, Inc.) to store and recall images in this sample. The basic optical setup is illustrated in figure 10. The total exposure necessary for writing a hologram with maximum diffraction effieciency was about 10 mJ/cm^2. With the 5 mwatts laser beam expanded to a size of about 5 cm^2, the exposure time necessary was about 10 seconds. Unfortunately, the *slowest* operating frame rate for our SLM (bought from Displaytech, Inc.) was 1 Hz. As such, we were not

able to use the SLM in the writing process. Instead, we used an air force resolution chart, placed just ahead of mirror 1 (see figure 10).

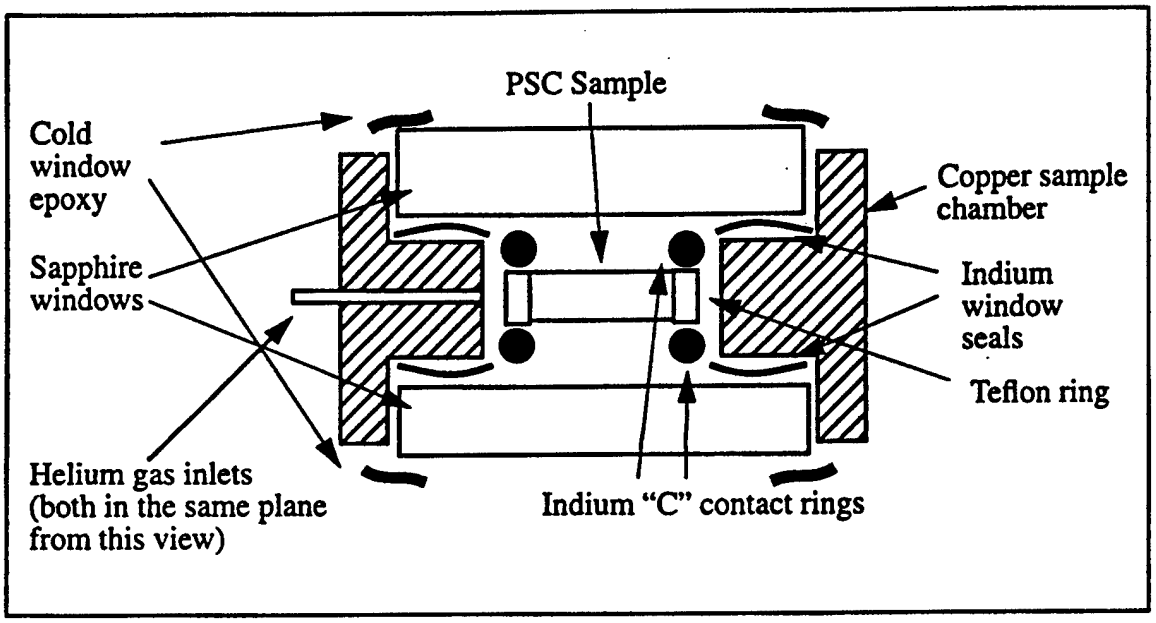

Figure 9. Cross-section view of the sample chamber in the helium cryostat.

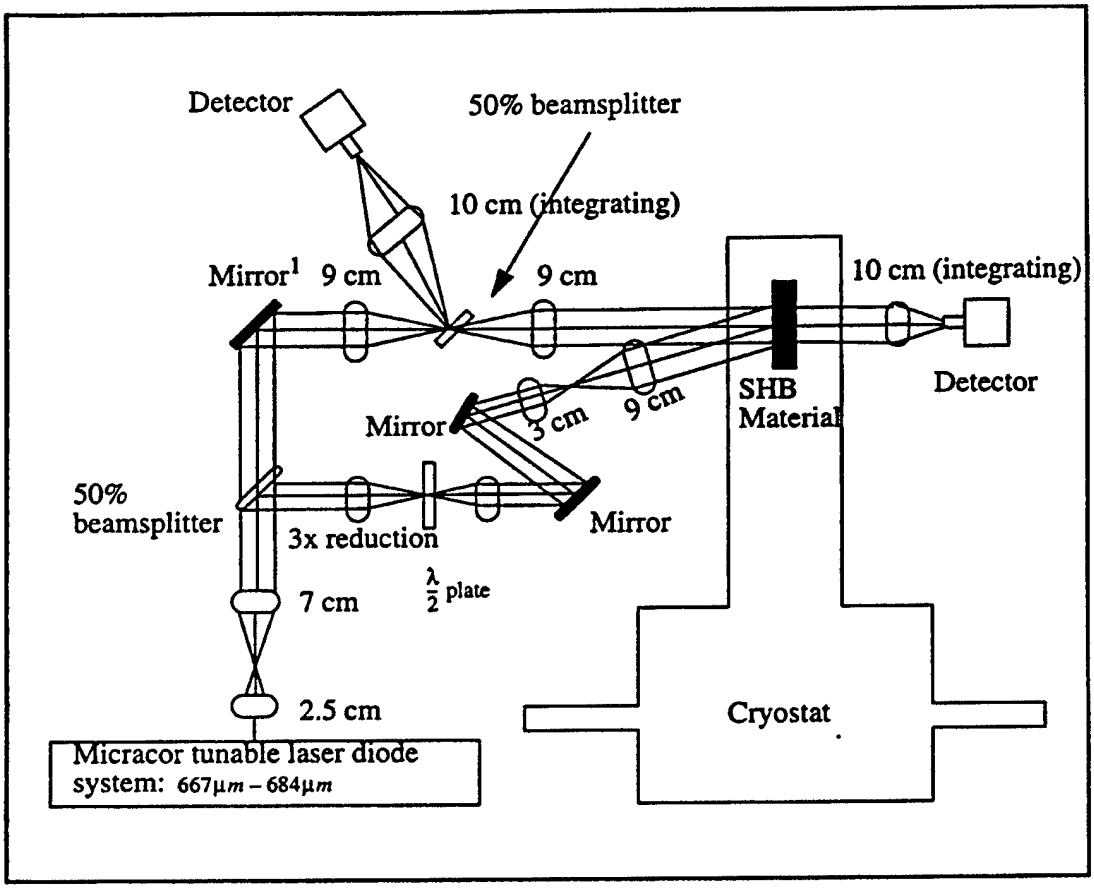

Figure 10. Schematic of the optical setup for writing images in the cryo-mounted PSC sample.

At 6K, we determined the inhomogeneous width of the PSC sample to be about 10 nm, and the homogenous width (i.e., the width of the spectral holes in the limit of low exposures) to be about 17 GHz. We wrote several angle multiplexed images at a given spectral whole, by varying the angle of the reference beam. The recorde images were then read back, and detected with a Cohu ccd camera. Two sample images retrieved from the recorded medium is shown in figure 11. As can be seen, the image quality is relatively poor, due primarily to imperfect optical quality of the sample; we also found that the sample suffered from a high level of scattering, with a fractional intensity of about $2X10^{-3}$.

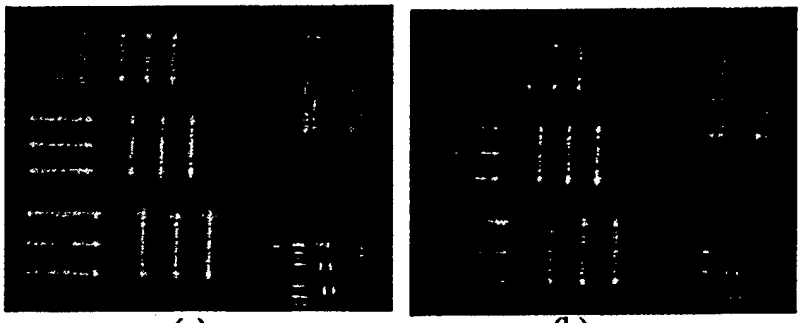

Figure 11. Two sample images retrieved from the PSC sample after recording.

Because of the rather high homogenoeus width, and the poor quality of the images, it is clear that we must explore another host medium. An attractive candidate material is PMMA, which is expected to have an inhomogenous width of about 15 nm, and a homogeneous width of about 1 GHz . In order to use PMMA as the host material, the key challenge again is the preparation of a dye-doped sample with smooth surfaces and low scattering. Recently, we have developed a special technique for prducing dye doped PMMA samples with optical quality surfaces, and a fractional volume scattering as low as $3X10^{-6}$. In such a sample doped with a dye called phenanthraquinone, we have demonstrated storage and recall of more than two thousand pages of video images at room temperature, using a galvo-scanned angular multiplexing . Figure 12 shows a sample image of the resolution chart, retrieved from a recorded sample of PMMA developed in our laboratory, along with the original image. As can be seen, the image quality is quite good. The methodology we have developed in this context will be used to create PMMA substrates doped with Chlorin-e_6.

ORIGINAL IMAGE #1

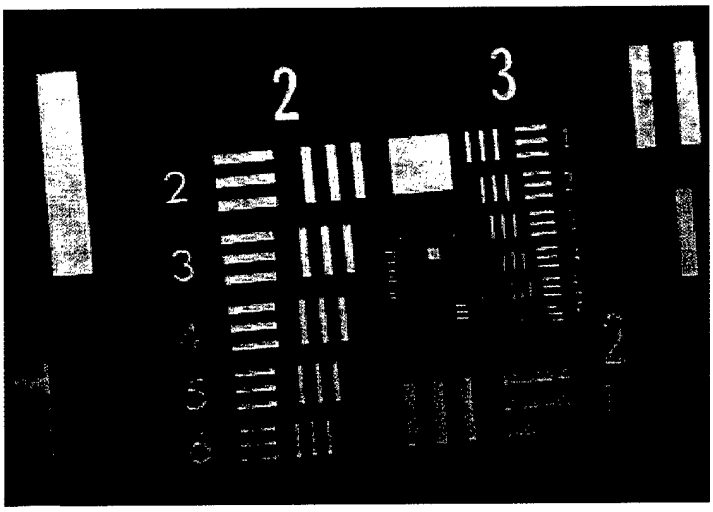

RECONSTRUCTED IMAGE #1

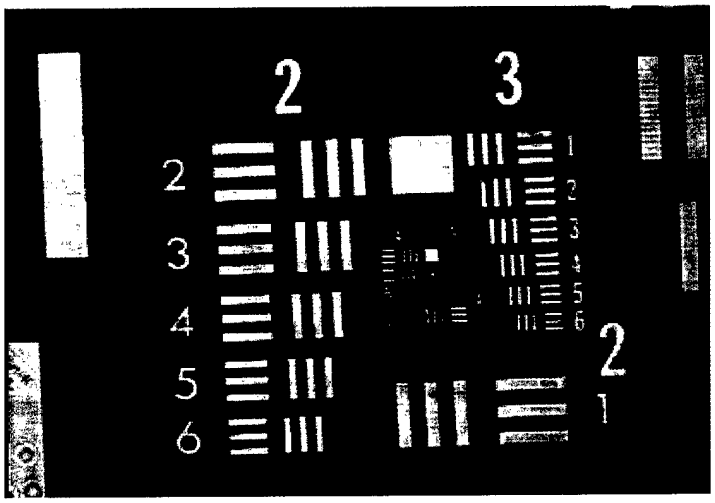

Figure 12: Comparison of the original with the holographic reconstruction of one of the ten images stored in a thick PMMA sample 5 mrads apart.

B.4 Observation of Electromagnetically Induced Transparency Above the Spectral-Hole-Burning Temperature Range

As information technology develops, not only large-capacity storage but also high-speed information processing is important for mass data communications. Recently, spectral hole-burning materials have attracted much attention because of potential applications in mass optical data storage, fast optical switches, and computing elements such as a dynamic random access memory module. For example, the usefulness of the hole-burning materials for high-density storage[1] and high-speed optical switches[2] has been already demonstrated using photon echoes.

In the spectral hole-burning media, the storage capacity is significantly increased by wavelength multiplexing using the large ratio of inhomogeneous to homogenous width for the optical transition. This wavelength multiplexing does not suffer from Bragg degeneracy caused cross-talk,[3] which limits storage capacity in volume holographic memories. That is because adjacent spectral holes are composed of different subsets of atoms, molecules, or ions.[4] In rare earth doped solids, the storage densities are $\sim 10^6$. This large storage density, however, is only available near liquid helium temperatures, because the optical homogenous width rapidly increases at higher temperatures due to phonon interactions.

Recently a spin echo memory excited by resonant Raman pulses, observed by us, has demonstrated the potential to overcome the temperature restrictions in the photon echo-based memories.[5] In the resonant Raman excited spin echo memory, it was shown that the spin coherence time T_2 (reciprocal of the homogeneous width) replaces the optical T_2 for the length of the write window. Thus, under ideal conditions, the memory density is determined by the ratio of the optical inhomogeneous width to spin, rather than the optical, homogeneous width. This is especially important for higher temperature applications, because the spin homogeneous width is less temperature sensitive. For example, we demonstrated the narrower and temperature insensitive spin homogeneous width in Pr^{3+} doped Y_2SiO_5 (Pr:YSO) up to 6K.[5]

For the efficient Raman excited spin echoes, electromagnetically induced transparency[6] (EIT) is an essential condition. In a three-level system interacting with Raman fields, EIT is caused by destructive quantum interference, so that the optically thick medium can be transparent. Recent demonstrations of EIT[7,8] and resonant Raman excited spin-echoes[5,9] in solids, however, still required near liquid helium temperatures. Here, we present an experimental observation of EIT in Pr:YSO at temperatures up to 15K well beyond the spectral hole-burning temperature. We show that the probe transmission increases by a factor of exp(1.4) at 12K.

Our system consists of 0.05 at. % Pr doped YSO in which Pr^{3+} substitutes Y^{3+}. For this work, the relevant optical transition is ${}^3H_4 \rightarrow {}^1D_2$, which has a frequency of ~ 606 nm. The inhomogeneous width of the optical transition is ~4 GHz at 1.4 K. The optical population decay time T_1 and transverse decay time T_2 are 164 μs and 111 μs, respectively at 1.4 K.[10] The ground (${}^3H_4$) and excited (${}^1D_2$) states have three degenerate hyperfine states, respectively. The splittings between the ground-hyperfine states are 10.2 MHz (±1/2 ↔ ±3/2), 17.3 MHz (±3/2 ↔ ±5/2), and 27.5 MHz (±1/2 ↔

±5/2).[10] The ground state spin decay times T_1 and T_2 are ~100 s[11] and 500 ms,[5] respectively, at 6 K for the 10.2 MHz transition. The spin inhomogeneous width for the 27.5 MHz transition is 80 kHz at 1.6K.[11]

Fig. 13 shows a schematic of the experimental setup. We use a frequency stabilized ring dye laser. The dye laser frequency jitter is about 2 MHz. For the resonant Raman transition, we excited the $^3H_4$ (±1/2) → $^1D_2$ (±3/2) transition with a coupling laser and the $^3H_4$ (±5/2) → $^1D_2$ (±3/2) transition with a probe laser. The coupling and probe fields are upshifted by 72.5 MHz and 100 MHz from the laser frequency, respectively. These fields are generated using acousto-optic modulators (AO) driven by frequency synthesizers (PTS 160). The probe field is fixed at resonance, while the coupling field is scanned across its resonance. The two laser beams are circularly polarized with a quarter wave plate and focused into the sample by a 25-cm focal length lens. The diameter (1/e in intensity) of the coupling laser beam is about ~ 50 μm in the crystal. The coupling laser intensity is varied up to a maximum of ~1.5 kW/cm^2. To produce laser pulses, we used rf switches driven by pulse generators. The pulse width is fixed at 50μs. A Boxcar averager averages 30 samples of the probe signal. The pulse repetition rate is 50 Hz. The angle between the coupling and probe fields is about 100 mrad. The spectral hole-burning crystal of Pr:YSO is inside a cryostat and its temperature can be varied. The size of the crystal is 3 mm×6 mm ×1 mm. Its optical B-axis is along the 1-mm length, and laser propagation direction is almost parallel to the optical axis.

Fig. 14 shows the probe absorption as a function of temperature. In Fig. 14, the coupling laser is blocked, and the probe intensity is adjusted not to saturate (over the temperature of the spectral hole burning). The power of the probe beam is 60 μW. Below ~8 K, the sample is nearly transparent to the probe because of spectral hole burning. The probe transmission rapidly decreases to ~10% at 10K. The minimum transmission of the probe is 4% at 20K. This high probe absorption continues up to ~25K and then gradually decreases. From the data in Fig. 2, the absorption coefficient α is calculated to be ~30/cm at the temperatures 12K - 20 K.

Fig. 15 shows the probe transmission versus the coupling laser detuning at 12K. The maximum coupling laser intensity is 1.2 kW/cm^2 in the crystal. At line center (Δ=0) of the coupling laser transition, the probe transmission is increased from 5% to 20 %, a factor of exp(1.4). The FWHM of the probe transmission increase is ~ 2.2 MHz. This width is much narrower than the optical homogeneous width at this temperature, which is deduced to be larger than 10.2 MHz, based on the assumption that the spectral hole-burning disappears when the the optical homogeneous width is larger than the ground state hyperfine splitting. This sub-natural linewidth in the probe spectrum (Fig. 15) is taken as evidence of EIT. Here, the efficiency of EIT is limited by available laser power. In previous work (Ref. 7), more efficient EIT was seen for lower coupling laser intensity, but the temperature was much lower. This is because the EIT efficiency is inversely proportional to the homogeneous width of the optical transition, which is broader at high temperatures.

In Fig. 16, we keep the temperature at 10 K, which gives partial spectral hole burning. Initially, the probe absorption is suppressed owing to EIT (see Fig. 15). When the coupling laser beam is switched off (at t=0 in Fig. 4), the probe beam absorption first increases and then gradually decreases. The absorption increase at t=0 is due to loss of

EIT; coherently trapped ions begin to absorb the photons. The absorption decrease afterward is because of the spectral hole burning. The spectral hole-burning saturation time depends on the strength of the probe.

Fig. 17 shows the probe transparency versus the coupling laser intensity. The temperature is fixed at 12 K. As expected, the probe transparency increases as the coupling laser intensity increases. The probe transparency increase is proportional to the square root of the coupling laser intensity. The coupling intensity axis is a log scale. For the data, the probe transparency is determined by the probe transmission change when the coupling laser is switched on.

In Fig. 18, we measured the probe transparency as a function of temperature with a fixed intensity of the coupling laser. As expected, the probe transparency decreases as the temperature increases. This is because the optical homogeneous width is broadened as the temperature increases, so that the EIT efficiency decreases. Over 15 K, we could not detect the EIT effect with our maximum coupling laser intensity of ~1.2 kW/cm^2.

To summarize this section, we have experimentally observed EIT in an optically thick, spectral hole-burning solid of Pr:YSO at higher temperatures than needed for spectral hole-burning. This demonstration is the first step toward implementation of high-density, high-speed optical memories based on resonant Raman excited spin echoes. The Raman excited spin echo memory can achieve the higher temperature memory applications, because the spin homogeneous width is less temperature sensitive than the optical width.

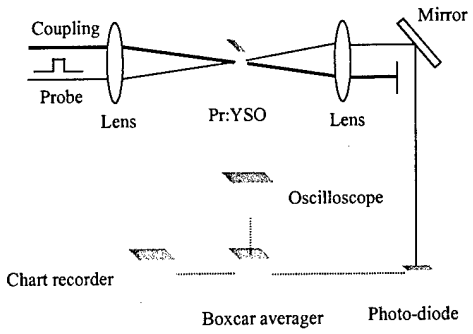

FIG. 13. Schematic of the experimental setup.

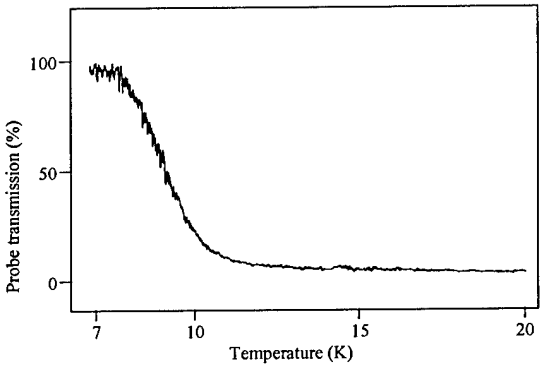

FIG. 14. Probe transmission versus temperature. The probe laser power is 60 μW.

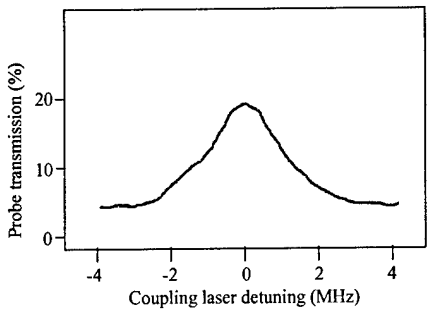

FIG. 15. Probe transmission versus coupling laser detuning at 12K.

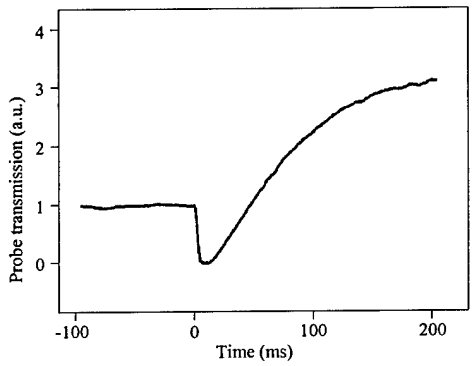

FIG. 16. Probe transmission versus time. At t=0, the coupling laser is off.

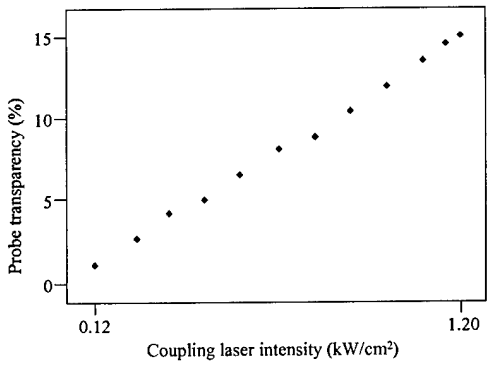

FIG. 17. Probe transparency versus coupling laser intensity.

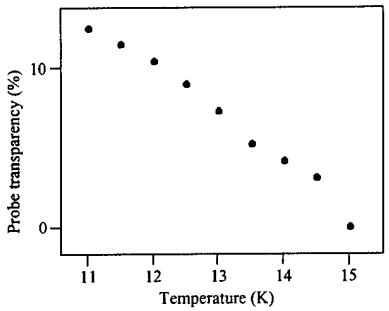

FIG. 18. Probe transparency versus temperature for fixed coupling laser intensity.

References

1. H. Lin, T. Wang, and T. W. Mossberg, "Demonstration of 8-Gbit/in.2 areal storage density based on swept-carrier frequency-selective optical memory," Opt. Lett. **20**, 1658 (1995).
2. X. A. Shen and R. Kachru, "Optical header recognition by spectroholographic filtering," Opt. Lett. **20**, 2508 (1995).
3. D. Psaltis, D. Brady, X.-G. Gu, and S. Lin, "Holography i artificial neural networks," Nature **343**, 325 (1990); A. Chiou, "Anisotropic corss talk in an optical interconnection by using a self-pumped phase-conjugate mirror at the Fourier plane," Opt. Lett. **17**, 1018 (1992).
4. U. P. Wild, S. E. Bucher, and F. A. Burkhalter, "Hole burning, Stark effect, and data storage," Appl. Opt. **24**, 1526 (1985).
5. B. S. Ham, M. S. Shahriar, M. K. Kim, and P. R. Hemmer, "Frequency-selective time-domain optical data storage by electromagnetically induced transparency in a rare-earth doped solid," Opt. Lett. **22**, 1849 (1997).
6. K. J. Boller, A. Imamoglu, and S. E. Harris, "Observation of electromagnetically induced transparency," Phys. Rev. Lett. **66**, 2593 (1991).
7. Y. Zhao, C. Wu, B. S. Ham, M. K. Kim, and E. Awad, "Microwave induced transparency in ruby," Phys. Rev. Lett. **79**, 641 (1997); B. S. Ham, P. R. Hemmer, and M. S. Shahriar, "Efficient electromagnetically induced transparency in a rare-earth doped crystal," Opt. Commun. **144**, 227 (1997).
8. B. S. Ham, M. S. Shahriar, P. R. Hemmer, "Enhanced nondegenerate four-wave mixing owing to electromagnetically induced transparency in a spectral hole-burning crystal," Opt. Lett. **22**, 1138 (1997).
9. B. S. Ham, M. S. Shahriar, M. K. Kim, P. R. Hemmer, "Spin coherence excitation and rephasing with optically shelved atoms," Phys. Rev. **B 58**, Rapid Comm. (In press).
10. R. W. Equall, R. L. Cone, and R. M. Macfarlane, "Homogeneous broadening and hyperfine structure of optical transitions in Pr3+:Y2SiO5," Phys. Rev. **B 52**, 3963 (1995).
11. K. Holliday, M. Croci, E. Vauthey, and U. P. Wild, "Spectral hole burning and holography in an Y2SiO5:Pr3+ crystal," Phys. Rev. **B 47**, 14741 (1993).

B.5 Enhancement of Four-wave Mixing and Line-narrowing Using Quantum Coherence in an Optically Dense Double-Λ Solid

Since the first proposal of enhanced nondegenerate four-wave mixing,[1] there have been several observations of the enhancement of nonlinear optical processes using two-photon coherence in gas media[2-7] and solids.[8] In particular, enhancement of the four-wave mixing generation in a Λ-type systems is found to be large under the conditions where coherent population trapping[9] plays an essential role.[5] Without two-photon coherence, four-wave mixing efficiency is lower on resonance, because the linear susceptibility $\mathrm{Im}(\chi^{(1)})$ competes with the nonlinear susceptibility $\mathrm{Re}(\chi^{(3)})$, and suppresses the nonlinear optical processes. However, using coherent population trapping or electromagnetically induced transparency,[8,10,11] the absorption can be suppressed even at the exact resonance. Recently, nondegenerate four-wave mixing was studied using double-Λ systems in atomic[5,6] and molecular[7] vapors. B. Lu *et al.* demonstrated higher four-wave mixing efficiency in a double-Λ system rather than in a single-Λ system using Rb vapor.[6]

Here, we report enhanced nondegenerate four-wave mixing using a double-Λ system in an optically thick spectral-hole-burning solid, Pr^{3+} doped Y_2SiO_5 (Pr:YSO). We have observed that the probe diffraction efficiency is 2.4 % in intensity (15.6 % in amplitude) at 6 K, which is higher than the efficiency (< 1 %) observed in a single-Λ system.[8,12] The observed diffraction efficiency using the double-Λ scheme in Pr:YSO is also higher than that observed in atomic[5,6] and molecular[7] vapors. High diffraction efficiency in a solid medium is important for potential applications such as optical memories,[12,13] high-resolution coherence spectroscopy,[14,15] lasers without population inversion,[16] and aberration correction.[17] We also report line narrowing of the four-wave mixing signal to below the inhomogeneous width of the sublevel transition. This line narrowing is due to the compression of two-photon transparency window in an optically dense medium.[15] The observed line-narrowing of the four-wave mixing signal has application to high-resolution spectroscopy.

Fig. 19 shows an energy level diagram of Pr:YSO. Our system consists of 0.05 at. % Pr doped YSO in which Pr^{3+} substitutes Y^{3+}. For this work, the relevant optical transition is ${}^3H_4 \rightarrow {}^1D_2$, which has resonant frequency of 606 nm. The inhomogeneous width of the optical transition is ~4 GHz at 1.4 K.[18] The optical population decay time T_1 and transverse decay time T_2 are 164 μs and 111 μs, respectively at 1.4 K.[18] The ground (${}^3H_4$) and excited (${}^1D_2$) states have three degenerate hyperfine states, respectively. The splitting between the ground-hyperfine states is 10.2 MHz (±1/2 ↔ ±3/2), 17.3 MHz (±3/2 ↔ ±5/2), and 27.5 MHz (±1/2 ↔ ±5/2).[18] The splitting between the excited-hyperfine states is 4.6 MHz (±1/2 ↔ ±3/2), 4.8 MHz (±3/2 ↔ ±5/2), and 9.4 MHz (±1/2 ↔ ±5/2).[18] The ground state population decay time T_1 is ~100 s,[19] and spin transverse decay time T_2 for the 10.2 MHz transition is 500 ms at 6 K.[12] The spin inhomogeneous widths for the 10.2 MHz transition is 30 kHz at 1.6 K.[19]

The laser fields of ω_1 and ω_2 in Fig. 19 act as pump beams, which create two-photon ground-state coherence via coherent population trapping. The laser field ω_P acts as a probe (read) beam, which scatters off on the two-photon coherence phase gratings

created by the pump beams, and generates the four-wave mixing signal ω_D satisfying phase matching condition $\mathbf{k_D}=\mathbf{k_1}-\mathbf{k_2}+\mathbf{k_P}$. The repump field ω_R is used to provide spectral selectivity in the otherwise inhomogeneously broadened system (~4 GHz inhomogeneous width). The amount of spectral selectivity provided by the repump depends on the laser jitter.

Fig. 20 shows a schematic of the experimental setup for the observation of nondegenerate four-wave mixing in Pr:YSO. We use a cw frequency stabilized ring dye laser pumped by a Ar-ion laser. The dye laser frequency jitter is about 2 MHz. We used acousto-optic modulators driven by frequency synthesizers (PTS 160) to make four different coherent laser beams as shown. For the resonant Raman transition, the pump beams ω_1 and ω_2 are downshifted by 60.0 MHz and 70.2 MHz from the laser frequency, respectively. The probe and repump field are downshifted from the dye laser output by 79.6 MHz and 47.3 MHz, respectively. All laser beams are linearly polarized and focused into the sample by a 30-cm focal length lens, so that the focused beam diameter (e^{-1} in intensity) is ~100 μm. The power of the pump lasers ω_1 and ω_2 is 12.5mW and 9mW, respectively. The power of the probe and repump lasers ω_P and ω_R is 18mW and 11mW, respectively. To produce laser pulses, we use rf switches driven by pulse generators. The pulse width of the pump and repump beams is fixed at 1 ms. The probe pulse width is 3μs and is delayed 2μs after the end of the pump and repump pulses. A Boxcar averager averages 30 samples of the four-wave mixing signal ω_D. The pulse repetition rate is 50 Hz. The angle between the pump and probe fields is about ~70 mrad. The spectral hole-burning crystal of Pr:YSO is inside a cryostat, and its temperature is fixed at 6 K. The size of the crystal is 3.5 mm×4 mm ×3 mm. Its optical B-axis is along the 3-mm length, and laser propagation direction is almost parallel to the optical axis.

Fig. 21 shows the efficiency of the four-wave mixing signal ω_D as a function of the detuning of the pump beam ω_2. The measured width (FWHM) is 97.0 kHz, which is two-photon power broadened. The maximum magnitude of the ω_D corresponds to a diffraction efficiency of 2.4 % in intensity. The actual conversion efficiency, however, must be higher because the beams do not copropagate and the sample is optically dense. In the limit of length l longer than beam overlapping length, the four-wave mixing signal intensity (I_D) is a function of time t and distance z, which depends on the two-photon coherence (ρ_{12}) induced by two pump fields:

$$I_D(l,t) \propto [\mathrm{Re}(\rho_{12}(z,t))]^2 \cdot I_P(0) \cdot \exp(-\alpha l) \qquad (1)$$

where z is between 0 and l, α is an absorption coefficient, and $I_P(0)$ is the probe intensity at z=0. In Eq. (1), the fact that four-wave mixing signal is proportional to the product of the pump intensities (until saturated) was demonstrated in atomic and molecular vapors.[6,7] This is because the two-photon coherence ρ_{12} is proportional to the product of pump Rabi frequencies (for weak pump beams). Using Eq. (1) and the absorption coefficient α~10 cm^{-1} of the sample, we can deduce that the actual conversion efficiency of the four-wave mixing is ~11 %, where we have replaced the crystal length l by effective length l'=1.5 mm based on 100 μm beam diameter and 70 mrad angle of intersection.

For comparison, we also used an off-resonant probe beam and observed maximum diffraction efficiency of less than 1% in intensity. This was observed when the probe beam frequency is detuned ~1 MHz from the pump beam ω_2.

To measure the minimum width of the two-photon coherence, we reduced the pump powers by factors of 100 and 10 for ω_1 and ω_2, respectively. Fig. 22 shows the resulting diffracted signal ω_D versus the detuning of the pump beam ω_2. Here, the pump pulses are lengthened to 5ms to increase the total pulse areas to compensate lower pump intensities. We also reduced the probe power by a factor of 2. The observed width (FWHM) of the four-wave mixing signal ω_D in Fig. 22 is 22.7 kHz, which is narrower by a factor of 1.3 than the inhomogeneous width (30kHz) of the 10.2 MHz transition. This line-narrowing is attributed to the compression of the two-photon transparency window in an optically dense medium. Such line-narrowing is explained by the effects of nonlinear dispersion on parametric processes in a dense phase-coherent medium.[15] In the Ref. 15, the line-narrowing is shown to be approximately proportional to the square root of optical density, which gives a factor of 1.2 using the effective length l' in our Pr:YSO. This is close to the observed narrowing.

To summarize this section, we have observed enhanced nondegenerate four-wave mixing generation using a resonantly probed double-Λ scheme in an optically dense spectral hole-burning solid. The measured diffraction efficiency is 2.4 % in intensity, and the conversion efficiency corrected for absorption is deduced to be ~11 %. This efficient four-wave mixing has potential application to nonlinear optical processes such as optical memories, high-resolution coherence spectroscopy, lasers without population inversion, and aberration correction. We also observed line-narrowing of the four-wave mixing signal. The observed line-narrowing is due to high optical density of the medium and is useful for the high-resolution spectroscopy.

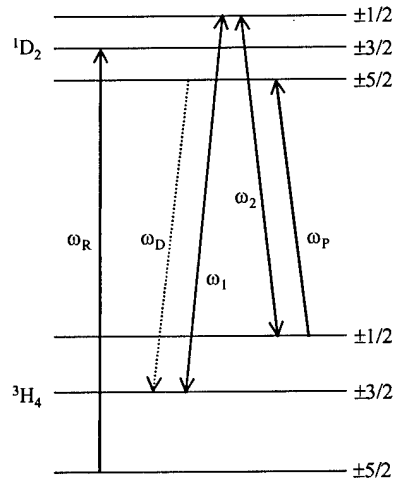

FIG. 1. Energy level diagram of Pr:YSO.

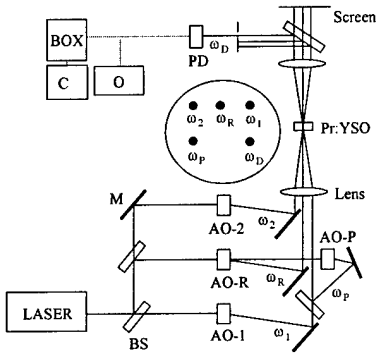

FIG. 2. Schematic of the experimental setup. AO, acousto-optic modulator; BOX, box-car integrator; BS, beam splitter; C, chart recorder; M, mirror; PD, photo-diode; O, oscilloscope. Inset: laser beams on screen.

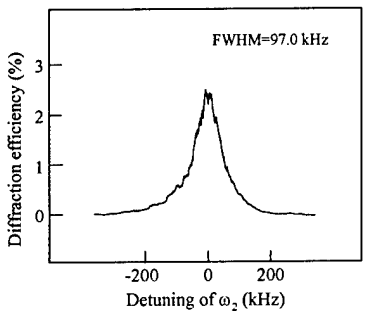

FIG. 3. Four-wave mixing signal efficiency at 6 K.

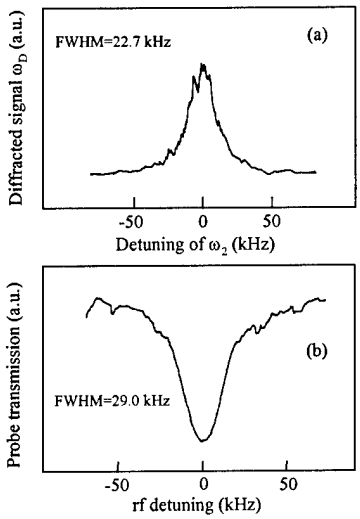

FIG. 4. Line narrowing of the four-wave mixing signal.

References

1. S. E. Harris, J. E. Field, and A. Imamoglu, Phys. Rev. Lett. **64**, 107 (1990).
2. M. Jain, G. Y. Yin, J. E. Field, and S. E. Harris, Opt. Lett. **18**, 998 (1993).
3. G. Z. Zhang, K. Hakuta, and B. P. Stoicheff, Phys. Rev. Lett. **71**, 3099 (1993).
4. Y. –Q. Li and M. Xiao, Opt. Lett. **21**, 1064 (1996).
5. P. R. Hemmer, D. P. Katz, J. Donoghue, M. Cronin-Golomb, M. S. Shahriar, and P. Kumer, Opt. Lett. **20**, 982 (1995).
6. B. Lu, W. H. Burkett, and M. Xiao, Opt. Lett. **23**, 804 (1998); Private communications for the conversion efficiency.
7. S. Babin, U. Hinze, E. Tiemann, and B. Wellegehausen, Opt. Lett. **21**, 1186 (1996).
8. B. S. Ham, M. S. Shahriar, and P. R. Hemmer, Opt. Lett. **22**, 1138 (1997).
9. H. R. Gray, R. M. Whitley, and C. R. Stroud, Jr., Opt. Lett. **3**, 218 (1978).
10. S. E. Harris, Phys. Today **50**, No.7, 36 (1997), and references therein
11. B. S. Ham, P. R. Hemmer, and M. S. Shahriar, Opt. Commun. **144**, 227 (1997); Y. Zhao, C. Wu, B. S. Ham, M. K. Kim, and E. Awad, Phys. Rev. Lett. **79**, 641 (1997);
12. B. S. Ham, M. S. Shahriar, M. K. Kim, and P. R. Hemmer, Opt. Lett. **22**, 1849 (1997).
13. B. S. Ham, M. S. Shahriar, M. K. Kim, and P. R. Hemmer, Phys. Rev. B **58**, Rapid Comm. (In Press).
14. Y. S. Bai and R. Kachru, Phys. Rev. Lett. **67**, 1859 (1991).
15. M. D. Lukin, M. Fleischhauer, A. S. Zibrov, H. G. Robinson, V. L. Velichansky, L. Hollberg, and M. O. Scully, Phys. Rev. Lett. **79**, 2959 (1997).
16. A. S. Zibrov, M. D. Lukin, D. E. Nikonov, L. Hollberg, M. O. Scully, V. L. Velichansky, and H. G. Robinson, Phys. Rev. Lett. **75**, 1499 (1995), and references therein.
17. V. S. Sudarshanam, M. Cronin-Golomb, P. R. Hemmer, and M. S. Shahriar, Opt. Lett. **22**, 1141 (1997).
18. R. W. Equall, R. L. Cone, and R. M. Macfarlane, Phys. Rev. B **52**, 3963 (1995).
19. K. Holliday, M. Croci, E. Vauthey, and U. P. Wild, Phys. Rev. B **47**, 14741 (1993).

C. Personnel Supported: We have supported two graduate students, both US citizens.

D. Publications:

Journal Publications

"Enhanced Nondegenerate Four-Wave Mixing Due to Electromagnetically Induced Transparency in a Spectral Holeburning Crystal," B.S. Ham, M.S. Shahriar, and P.R. Hemmer, *Opt. Letts* **22,** 1139(1997).

"Efficient Electromagnetically Induced Transparency in a Rare-Earth Doped Crystal," B.S. Ham, P.R. Hemmer, and M.S. Shahriar, *Opt. Commun.* **144,** 227(1997).

"Frequency Selective Time Domain Optical Data Storage by Electromagnetically Induced Transparency in a Rare-earth Doped Solid," B.S. Ham, M.S. Shahriar, M.K. Kim, and P.R. Hemmer, *Opt. Letts.* **22,** 1849(1997).

"Ultra-high Density Optical Data Storage," M.S. Shahriar, L. Wong, M. Bock, B. Ham, J. Ludman, and P. Hemmer, *Symposium on Electro-Optics: Present and Future*, 1998 Optical Society of Americs book series on *Trends in Optics and Photonics.*, H. Haus, ed., pp 97-104.

"Radio-frequency Induced Optical Gain in Pr:YSO," B.S. Ham, P.R. Hemmer, and M.S. Shahriar, *J. Opt. Soc. Am. B.* **15,** 1541 (1998).

"Spin Coherence Excitation and Rephasing with Optically Shelved Atoms," B.S. Ham, M.S. Shahriar, and P.R. Hemmer, *Phys. Rev. B* **58** R11825 (1998).

"RF Coupled Optical Gain in a Solid Owing to Quantum Interference," B.S. Ham, M.S. Shahriar, and P.R. Hemmer, *Optics and Photonics News,* Dec. 1998.

"Enhancement of Four-wave Mixing and Line-narrowing Using Quantum Coherence in an Optically Dense Double-Λ Solid". B.S. Ham, M.S. Shahriar, and P.R. Hemmer, *Opt. Letts.* **24,** 86 (1998).

"Quantum interference and its potential applications in a spectral hole-burning solid," B.S. Ham, M.S. Shahriar, P.R. Hemmer, and M.K. Kim, *Laser Physics* **9,** No. 3 (1999).

"Electromagnetically induced transparency over spectral hole-burning temperature in a rare-earth-doped solid," B.S. Ham, M.S. Shahriar, and P.R. Hemmer, *JOSA B* **16,** No. 5 (1999).

"Observation of Laser-Jitter-Enhanced Coherence Spectroscopy and Spin Spectral Hole Burning in an Inhomogeneously Broadened Medium," B.S. Ham, M.S. Shahriar, and P. Hemmer, to appear in *Opt. Commun.* (2000)

Conference Publications

B.S. Ham, P.R. Hemmer, and M.S. Shahriar, "Observation of Enhanced Non-Degenerate Four Wave Mixing and Efficient Electromagnetically Induced Transparency in an Optically Dense Rare-Earth Doped Crystal," OSA Annual Meeting Technical Digest 1997 (Opt. Soc. of Am., Washington, D.C.,1997).

B.S. Ham, M.S. Shahriar, P.K. Kim, and P.R. Hemmer, "Optical Data Storage by Electromagnetically Induced Transparency and Nondegenerate Four-wave Mixing in a Spectral Hole-burning solid," Conference on Lasers and Electro Optics, May 1998, San Francisco, CA.

B.S. Ham, P.R. Hemmer, and M.S. Shahriar, "Optical Memory using Resonant Raman Excited Spin Echoes," OSA Optical Data Storage Topical Meeting, May 1998, Aspen, CO.

B.S. Ham, P.R. Hemmer, and M.S. Shahriar, "RF-induced Gain of Laser Beams in an Optically Dense Rare Earth Doped Solid," OSA Annual Meeting, 1998, Baltimore, MD.

M.S. Shahriar, B.S. Ham, V.S. Sudarshanam, and P.R. Hemmer, "Nonlinear Optics in Resonant Systems Applied to Signal Processing," the OSA Annual Meeting, 1998, Baltimore, MD **(invited)**

B. Ham, M.S. Shahriar, and P.R. Hemmer, ""Efficient Phase Conjugation using Raman dark resonances in an optically dense solid," Conference on L asers and Electro-Optics, Baltimore, MD, 1999.

B. Ham, M.S. Shahriar, and P.R. Hemmer, ""Electromagnetically induced transparency over spectral hole-burning temperature in an inhomogeneously broadened solid," Conference on L asers and Electro-Optics, Baltimore, MD, 1999.

B. Ham, M.S. Shahriar, and P.R. Hemmer, "Observation of Laser Jitter Enhanced Hyperfine Spectroscopy," OSA Annual Meeting, Santa Clara, CA, 1999.

B. Ham, M.S. Shahriar, and P.R. Hemmer, "Enhancement of Four-wave-mixing and Line-narrowing using EIT in an optically dense double-lambda solid," OSA Annual Meeting, Santa Clara, CA, 1999.

M.K. Kim, B. Ham, M.S. Shahriar, and P.R. Hemmer, "Sub-kHz resonance structure in rf-optical double resonance of rare-earth ions in solids," OSA Annual Meeting, Santa Clara, CA, 1999.

New discoveries, inventions, or patent disclosure: None